Composites Communications 63 (2026) 102747

Contents lists available at ScienceDirect

Composites Communications

journal homepage: www.elsevier.com/locate/coco

Design of integrally 3D-printed sandwich structures with functionally graded honeycomb and continuous carbon fibre-reinforced grid hybrid cores

Itxaro Sukia *, Aritz Esnaola, Unai Morales, Jon Aurrekoetxea

Mechanical and Industrial Production Department, Mondragon Unibertsitatea, Loramendi 4, 20500, Mondragón, Spain

ARTICLE INFO

Keywords:
Bio-inspired sandwich
3D printed composites
Functionally graded structure
Topology optimisation
Continuous-fibre composites

ABSTRACT

Sandwich structures are critical for lightweight engineering yet preventing face–core interface failure remains a significant challenge. Additive manufacturing offers a solution by enabling complex, integrally reinforced designs, though optimising these for mechanical performance requires advanced strategies. To address this, this study demonstrates the feasibility of manufacturing fully 3D-printed sandwich panels using material extrusion, featuring a tree-leaf-inspired honeycomb–grid hybrid core. The proposed multi-scale design approach involved three steps: (i) topology optimisation to generate a material distribution map; (ii) construction of a cellular structure with varying trabecular cell sizes; and (iii) integration of a curved grip mesh at domain boundaries to ensure geometric and mechanical continuity. Incorporating the grid into the functionally graded core improved strength by 4%, while embedding continuous carbon fibres further increased strength by 52%. The benefits of fabricating the sandwich panel in a single printing step using polyamide for both face sheets and cores include larger adhesion areas and reduced stiffness mismatch. Failure analysis revealed a shift in failure mode from the core–face interface to the face sheets themselves, indicating enhanced structural integrity. These findings highlight the potential of hybrid 3D-printed sandwich structures for lightweight, high-performance applications.

1. Introduction

The aerospace [1,2] and automotive [2] industries extensively use sandwich panels as lightweighting solutions because their high specific stiffness and strength, combined with the ability to absorb impact energy and provide thermal insulation, make them highly versatile for meeting specific product requirements [3]. These structures offer a wide range of design options, including face sheet materials such as composites or lightweight alloys, different types of cellular cores [3] and bio-inspired face sheet architectures [4]. This versatility provides a broad spectrum of optimisation solutions for structural engineers.

Cellular cores are generally classified into two main groups: stochastic cells (random microstructures found in foams) and periodic cells [5]. Periodic cells include two-dimensional varieties such as honeycombs and corrugated materials, and three-dimensional lattice structures. Hexagonal cells, frequently found in honeycomb cores, are the most common unit cell type in structural sandwich panels [3]. However, recent advancements in bio-inspired core designs have captured significant attention due to their remarkable mechanical properties [6]. After comparing natural cell concepts published in the literature, Ha and Lu [7] identified the trabecular structure of a beetle's forewing as the most efficient unit cell. In fact, Yu et al. [8] investigated various design configurations to tune the stiffness of sandwich core structures inspired by these trabecular cells, aiming to broaden their potential applications. The choice of infill pattern and core architecture remains a critical factor for performance, particularly under dynamic loading where specific cell designs can significantly enhance energy absorption and impact resistance [9]. Functionally graded (FG) structures [6], where cell size and wall thickness vary locally to accommodate specific loads, represent another innovative design strategy derived from natural principles.

Several studies on bio-inspired designs have also highlighted the potential of mimicking the hierarchical structures of tree leaves to improve the strength, stiffness, and toughness of sandwich structures [10–14]. The fractal vein distribution in tree leaves, with primary and secondary veins of varying thickness and length, serves as a model for optimising core designs. The most explored concept combines a periodic aluminium orthogrid (acting as primary thick veins) with aluminium honeycomb blocks (acting as secondary thin veins). Shi et al. [10,11]

* Corresponding author.
E-mail address: isukia@mondragon.edu (I. Sukia).

https://doi.org/10.1016/j.coco.2026.102747
Received 16 June 2025; Received in revised form 21 January 2026; Accepted 2 February 2026
Available online 4 February 2026

studied the three-point bending behaviour of such cores with carbon-fibre reinforced composite thin face sheets, demonstrating significant enhancements in specific flexural strength and energy absorption [10]. Additionally, substituting the aluminium grid with a carbon-fibre reinforced composite grid can further improve specific stiffness, despite higher manufacturing costs [11]. Sun et al. [12,13] showed that sandwich structures with a honeycomb–grid hybrid core significantly outperform single-core designs in terms of stiffness, critical load, and damage tolerance. This enhanced performance is attributed to the increased interfacial contact area from the honeycomb and the high moment of inertia from the grid, which effectively prevents interfacial debonding and local buckling. Furthermore, parametric studies on impact resistance [14] revealed that grid thickness is the most influential factor, significantly enhancing peak load and reducing internal damage.

Designing a trabecular core with a cell size distribution adapted to complex loading scenarios, such as twist-bending, and determining the design of the grid-structure are not trivial engineering tasks. Topology optimisation (TO) algorithms provide a robust mathematical framework for conceptualising these designs. Casalotti et al. [15] introduced an innovative multi-scale design strategy for architected composite structures, using to translate global density maps into local architected features. The methodology begins with a comprehensive definition of the initial problem, including the geometry, conditions, and applied loads on the structure. This approach enables the design of functionally graded (FG) cores that are specifically reinforced where high shear or tensile stresses occur, maximising the structural efficiency of the CFRP-AM components. The final step involves a de-homogenization process to retrieve the final cellular structure, strategically allocating hexagonal cells with varying dimensions across different regions.

Traditional honeycomb manufacturing technologies are optimised for producing uniform cellular and flat products; complex shapes must be machined or thermoformed, increasing costs [3]. A critical challenge in these conventional panels is the face sheet–core interface, which is often the weakest point due to the small bonding area and high stiffness mismatch. However, embedding a grid within the honeycomb has been shown to reduce this mismatch [10]. Another innovation driver is the growing environmental concern, leading manufacturers to opt for fully thermoplastic sandwich panels [16] for their recyclability compared to thermoset composites or Nomex® cores. While novel strategies involving continuous fibre 3D-printed thermoset honeycombs with foam reinforcement are being explored [17], thermoplastic material extrusion (MEX) is an emerging technology that facilitates the use of both unreinforced plastics and continuous fibre-reinforced composites (CFRP-AM) in the same 3D printing process [18]. This versatility presents significant design opportunities [19], though it necessitates robust strategies for joints and interfaces to maintain structural continuity [20]. Crucially, the mechanical performance of these structures is governed by the material properties. As reported in the literature [21,22] the ply and interlaminar behaviours of 3D-printed continuous carbon fibre-reinforced thermoplastic laminates are highly sensitive to processing conditions and the generated microstructure.

Current research on additively manufactured cores primarily follows two approaches: adhesively bonding face sheets onto the core [23–25], or integral 3D printing of the entire sandwich structure. While adhesive bonding mirrors conventional manufacturing challenges—such as interface debonding and weight penalties—integral printing enhances the interface strength by ensuring material continuity and reducing stiffness mismatch [26–28]. Unit cell orientation is a critical factor in sandwich production. For sandwich structures with corrugated cores, the main axis of the cells is perpendicular to the build orientation, eliminating the need for support structures. Sugiyama et al. [26] demonstrated that using continuous fibres in the printing of facings offers a notable advantage. The tension generated during fibre extrusion allows the material to effectively span the cell gaps, eliminating the need for support structures in enclosed geometries.

A comprehensive review of the literature reveals that bio-inspired, functionally graded, integrally 3D-printed sandwich structures with honeycomb–grid hybrid cores are currently in an early stage of development, and reported load cases are often overly simplistic. In this paper, we compare the stiffness of three beetle-forewing-inspired sandwich structures: (i) a functionally graded core, (ii) the same graded core with a boundary grid placed along the interfaces between domains of different cell sizes, and (iii) the graded core with the boundary grid reinforced by continuous carbon fibre. The graded cell-size distribution is obtained by mapping a topology-optimisation solution for a combined twisting–bending (plate-twist) load case, and the grid enforces geometric and mechanical continuity across domains. All panels are manufactured integrally in a single material-extrusion build, using polyamide reinforced with micro carbon fibres for the core and face sheets, and continuous carbon fibre for the grid.

2. Methodology

2.1. Materials and manufacturing

Sandwich panels were manufactured in a single step (integral 3D printing) using two PA-based filaments from Markforged®: Onyx® (PA6 with ≈11 vol% micro carbon fibres) and cCFPA (PA reinforced with ≈36 vol% continuous carbon fibres). The quantitative properties used in this work are those reported in Table 1 (from Ref. [29]) and are used consistently throughout the analysis. Datasheet ranges for the same materials typically report: Onyx® density ≈1200 kg/m^3, tensile modulus ≈1.4–2.4 GPa, tensile strength ≈30–40 MPa; continuous-carbon-fibre composites (UD plaques) tensile modulus ≈ 54–60 GPa, tensile strength ≈ 700–800 MPa. Printed-part performance depends on fibre paths, lay-up, and process conditions; therefore, Table 1 remains the sole quantitative source in this study.

A Mark Two (Markforged®) with dual extrusion was used—one head deposited Onyx®; the second placed continuous carbon fibre into designated paths. Supplier default parameters were used for both materials. We selected 100% infill and 0.125 mm layer height. The first and last two face-sheet layers were printed in Onyx® to ensure surface finish.

Core cells were oriented perpendicular to the print bed, and face sheets parallel to it. Continuous fibres were placed along the boundary grid between domains of different cell sizes to enforce geometric/mechanical continuity. Fig. 1 shows the build chamber and the adopted orientation; this configuration helps avoid internal supports within enclosed sandwich geometries. Prior composite-AM work also reports that fibre tension can bridge cell openings, enabling support-free printing in such setups. All parts were processed dry (polyamide-based filaments) and conditioned at 23 °C, 50 % RH for 4 days prior to testing.

2.2. Sandwich panel design

The method for designing the functionally graded honeycomb-grid hybrid core was based on the approach proposed by Casalotti et al. [15] (Fig. 2). First, based on the design space and load conditions (structural problem), topology optimisation software (Inspire®) was used to propose the solid design with the material distribution (optimised topology). Simultaneously, the properties of the trabecular cells with different side lengths were characterised, and the optimal cell sizes for the core were selected (architecture choice). In the second step, the core was reconstructed using varying cell sizes according to the material

Table 1
Mechanical properties of the materials for 3D printing [29].

	Density [kg/m^3]	Elastic Modulus [GPa]	Tensile strength [MPa]	Break strain [%]
Onyx®	1180	1.2	53	38
cCFPA	1250	69.4	905.3	1.27

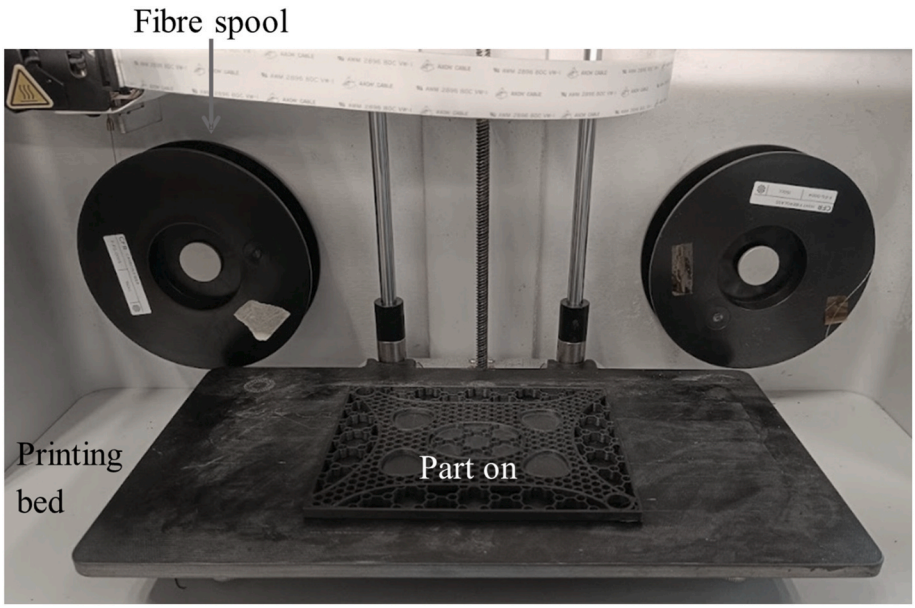

Fig. 1. Build view and integral manufacturing concept.

distribution (architecture cellular core design). Subsequently, a grip structure was incorporated along the boundaries between domains with different cell sizes (grid core design), simulating a tree-leaf microstructure [10–14]. The grid (2.7 mm width) is co-printed with the core and, in the FG_CF variant, hosts continuous carbon fibres to enhance load transfer across domains. Finally, the face sheets were added to the sandwich.

2.2.1. General description

The sandwich panel measured 155 mm × 122 mm and was rectangular in shape. The symmetrical face sheets had a thickness of 1.5 mm with a quasi-isotropic $[0/90/45/-45]_2$ lay-up. The core, made of Onyx®, had a thickness of 10 mm. The load case for optimising the core design involved a two-point plate twist. In this setup, the rectangular plate was supported by bolts in cylindrical holes located at the corners of one diagonal, while a 100 N force was applied to each corner of the opposite diagonal using two hemispheric heads, each with a diameter of 20 mm. This load case, inspired by the test method proposed by Aviles et al. [30], is more complex than the previously used cases, which primarily involved beams under three-point bending. It presents a non-trivial optimised proposal, offering a better understanding of the potential of combining topology optimisation with additive manufacturing in sandwich panel design.

2.2.2. Topology optimisation of the embodiment solid design

The design space encompassed the entire core volume, excluding the surfaces of the cylindrical holes used for supporting the sample. The upper and lower face sheets were excluded from the topology optimisation study. The design space was discretised with a 0.5 mm mesh size, and the SIMP method assigned a density value to each element, either 0 or 1. A value of 0 indicated that material could be eliminated, while a value of 1 denoted that material was needed at that position. For intermediate density values, the software rounded them to either 1 or 0. The objective of the optimisation was to maximise stiffness while reducing mass to 30%, applying a safety factor of 3. Given the high degree of flexibility permitted by the manufacturing process, no constraints were imposed. The topology-optimisation load case equals the experimental plate-twist boundary conditions shown in Fig. 3 (two bolted supports on one diagonal and two Ø20 mm hemispherical heads applying F each on the opposite diagonal).

2.2.3. Architecture choice: unit cell size selection

The forewing of the beetle served as the inspiration for the unit cell of the core, which was the trabecular structure [7]. This structure is characterised by a ratio of the cylindrical column diameter to the length of the side (L) of 0.5 and a wall thickness of 0.7 mm [31]. Based on the overhang test results reported by Sugiyama et al. [26], the biggest cell size studied was 10 mm side length, being the smallest 3 mm length (Table 2).

2.3. Mechanical characterisation tests

All experimental characterisation is reported in this section. We evaluate core-level behaviour via flatwise compression (ASTM C365/C365M) and plate-twist loading, and sandwich-level behaviour via the same plate-twist boundary conditions shown in Fig. 3.

The out-of-plane compression performance of cells with different sizes was characterised in accordance with ASTM C365-16. Following the recommendations of this standard, which suggests using different sample sizes depending on the core density, samples with two different diameters were 3D printed: 58 mm for structures with a cell side length of 6 mm or less, and 86 mm for the others. All samples had a height of 10 mm. The tests were conducted using a Hoytom/HM-D universal testing machine equipped with a 100 kN load cell, in a room maintained at 23 °C and 50% relative humidity. The elastic modulus (E) and strength (σ_c) were calculated using data from the experimental curves and the equations proposed in ASTM C365-16. The energy absorption (EA) and specific energy absorption index (SEA) were calculated by dividing the area under the stress-strain curve up to the densification point, identifying this critical strain by truncating the curve at the same load level as the first peak [32]. Three samples of each core structure type were tested to calculate average values and standard deviations for each property.

The method of testing the twist plate was proposed by Aviles et al. [30] and is based on the ASTM D3044 for shear modulus of wood-based structural panels. Aviles modified the standard for other sizes of panels and for sandwich structures. The compliance of the specimen (C) is defined as the displacement of each loading point (δ) divided by the applied load (F). $C = \delta/F$. Applying the standard, the compliance expression leads to,

$$C = \frac{ab}{16D_{66}}$$

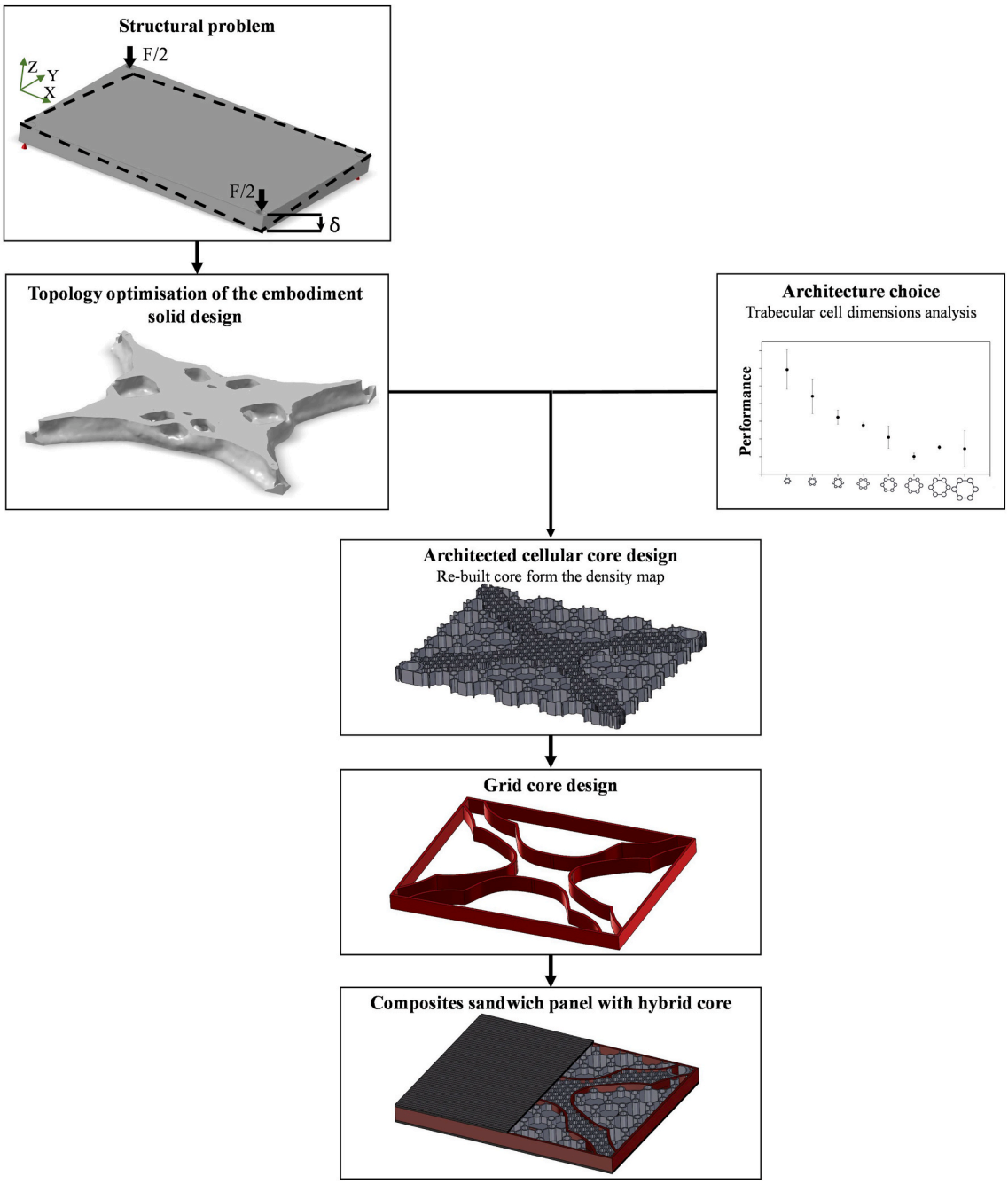

Fig. 2. Schema of the followed methodology.

Where, a and b are the panel dimensions, D_{66} is the twist stiffness.

Performance comparisons of the different design variants were conducted based on the load case used for the topology optimisation (Fig. 2), which is particularly well-suited to characterizing the behaviour of sandwich structures [30], plate twist test. Tests were conducted at a speed of 1 mm/min using the same equipment as the compression test. Displacement was directly recorded from the testing machine's moving head, while the load was measured by the load cell. The experiments were conducted at 23 °C and 50% relative humidity. Three samples of each type were 3D printed and subjected to this experimental procedure, which was applied to both the cores and sandwich panels.

3. Results and discussion

3.1. Sandwich plate design

3.1.1. Topology optimisation of the embodiment solid design

Topology optimisation software was employed to determine a material distribution that would be more suitable for the twist bending load case, with the objective of maximising the stiffness of the panel, with a volume fraction constraint of 30%. Fig. 4 illustrates the solution that the software proposed for the upper (Fig. 4b) and lower (Fig. 4c) part of the panel. It can be seen that the material is concentrated in an elliptical region at the centre of the plate, connected by four pyramidal arms to the assembly and loading corners. It is crucial to highlight that the material distribution differs between the upper and lower views of the core in order to more effectively carry the compression and tensile loads.

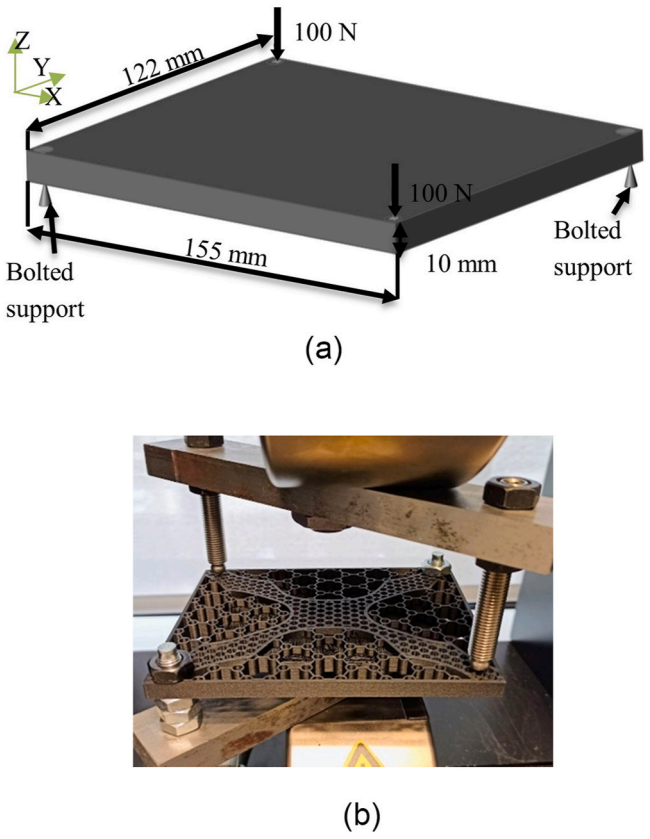

Fig. 3. (a) Plate-twist boundary conditions and coordinate system used in both topology optimisation and experiments. (b) Real photo of the actual test setup showing the specimen, heads, supports and measurement points.

Table 2
Density and relative density values of the studied compression samples.

Sample	L3	L4	L5	L6	L7	L8	L9	L10
ρ [kg/m^3]	464	380	312	245	216	193	170	160

Finally, the design proposes empty domains embedded in the arms and central region that must be taken into consideration when redesigning the panel and applying the functionally graded design.

From a functional graded core design perspective, the material distribution consists of completely solid or empty domains, without zones of intermediate densities. Therefore, for the analysed loading scenario, two cell sizes may suffice: the smaller size for areas with structural significance, and the larger for regions where material is not required but must serve as support for the top face sheet during 3D printing.

3.1.2. Architecture choice

The architecture choice is guided by (i) ASTM C365 compression-derived stiffness, strength, energy absorption and *SEA* for printable cell sizes, and (ii) plate-twist compliance/stiffness under the boundary conditions of Fig. 3. The analysis of the out-of-plane compression tests for different cell sizes was conducted using stress-displacement curves to determine the stiffness, strength, and specific properties of each structure. Fig. 4a shows the representative curves for each cell size. According to Bhat et al. [33,34], each curve can be divided into three regions corresponding to the deformation stages.

The first region corresponds to linear elastic strain in the cell walls. However, as the load increased, this linearity was lost. For samples L4 through L10, a distinct peak force was reached followed by a drop, attributed to the onset of cell buckling. The absence of a distinct first peak and stress drop in L3 samples (the densest cells) highlighted that macroscopic buckling or fracture mechanisms were suppressed or delayed due to the high relative density.

The second region is the plateau region, where the structure undergoes plastic deformation. Following the classification by Ashby et al. [35], the shape of the stress-strain curve in this region indicates the dominant failure mode: a convex curve with a decreasing slope represents stretch-dominated behaviour, while a constant or increasing slope indicates bending-dominated behaviour. In the present study, a convex curve was observed for all cell sizes, indicating that the main failure mechanism is brittle buckling or fracture. This is visually confirmed in Fig. 5b, which illustrates the real compression deformation stages (elastic, buckling/fracture, and densification). The correlation between the convex drop in stress and the physical collapse of the cell walls confirms the brittle nature of the failure.

The third region is the densification stage, characterized by a rapid increase in stress. In this study, the tests were terminated when the stress in the densification phase reached the value of the initial peak.

As a general rule, increasing the trabecular cell side length L produces a monotonic decrease in all measured properties—compressive modulus *E*, specific strength, energy absorption (*EA*) and specific energy absorption (*SEA*)—followed by a clear plateau for $L > 7$–8 mm (Fig. 6). In stiffness (Fig. 6a), the most pronounced drop occurs between L3 and L6; for L7–L10 the values cluster around a plateau within the error bars. Specific strength (Fig. 6b) shows the same two-regime behaviour. *EA* (Fig. 6c) decreases with *L* in parallel with *SEA* (Fig. 6d); however, because specimen mass varies with *L*, *SEA* is used as the primary metric for cross-size comparison, with *EA* reported alongside for structure characterisation. These trends are consistent with the stretch-dominated crushing described above: increasing *L* lowers the effective load-bearing wall density and increases wall slenderness, promoting earlier local buckling/brittle failure; once that mechanism fully governs, further increases in *L* have little additional effect. Based on these results, small cells (e.g., L3–L4) are preferred for high-demand regions of the graded core, while large cells (e.g., L10) are adequate in low-demand regions.

3.1.3. Architected cellular and grid core design

Based on the criteria outlined in Section 3.1.1 and the results in Section 3.1.2, the trabecular cell with L3 was selected for the dense domains due to its higher stiffness, strength, and *(S)EA*. For low-demand regions, the L10 cell was chosen since it maintained the mechanical performance observed for larger cells while reducing printing time by ~19% compared with L8. Distributing L3 and L10 according to the material-distribution map (Fig. 4) yielded the functionally graded (FG) core. To adapt the core to the twist-bending case, the architecture is split through the thickness into two functional halves: the upper half (tension side under plate-twist) and the lower half (compression side), separated by a 0.5 mm interface plate to ensure geometric and mechanical continuity across changes in cell size. The mapping from the topology solution to the architected lattice is shown by superposition in Fig. 7: (a) upper half and (b) lower half overlays make explicit how dense (L3) and sparse (L10) domains follow the optimised load paths. Photographs of the corresponding printed halves are shown in Fig. 7c and d.

By mapping the selected trabecular cells (L3 and L10) onto the optimised stress paths identified in Section 3.1.1, the final FG core achieved a real density of approximately 386 kg/m^3. This implementation demonstrates how the theoretical weight reduction target of 30% was translated into a physical cellular architecture that prioritizes material in high-stress domains while minimizing mass in low-demand regions.

As detailed in the design workflow (Section 2.2), a boundary grid is placed along the interfaces between domains of different cell sizes. The grid width is 2.7 mm—the minimum needed to host a continuous-fibre bed—so it can be co-printed in a single build with the core and face sheets. This enables three core variants used later for comparison: (i) FG_noGrid (graded cells only), (ii) FG (graded cells + Onyx® boundary

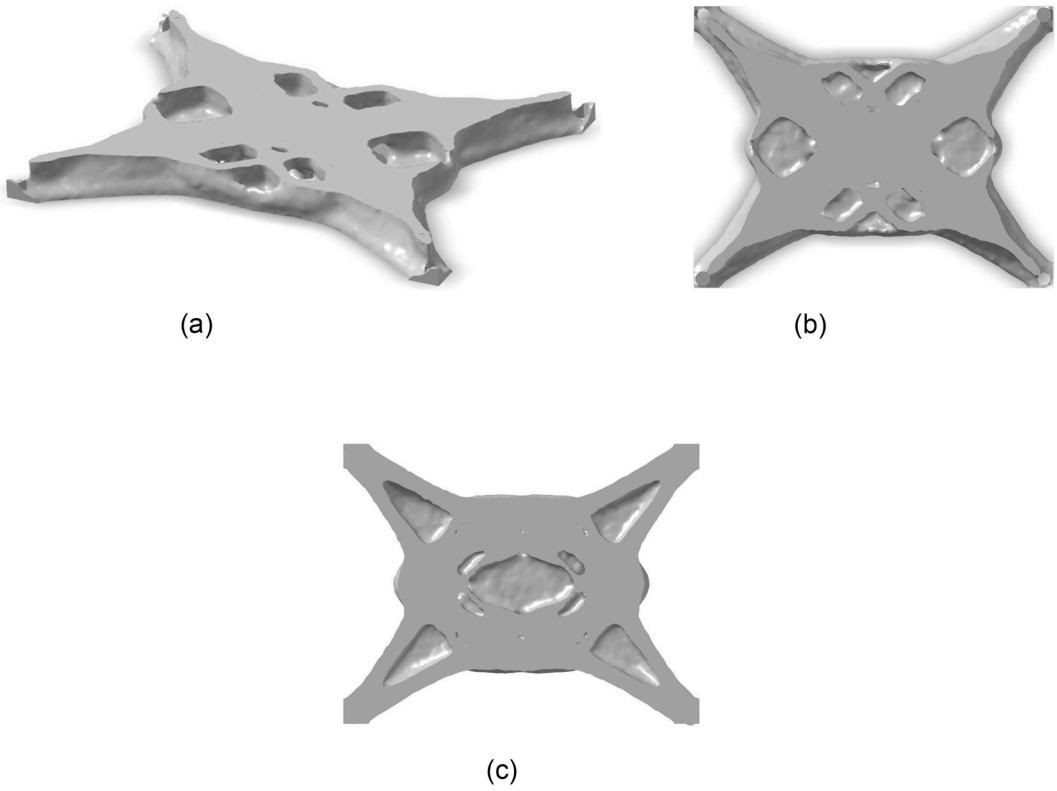

Fig. 4. Topology optimisation material distribution: isometric (a), upper (b) and lower view (c).

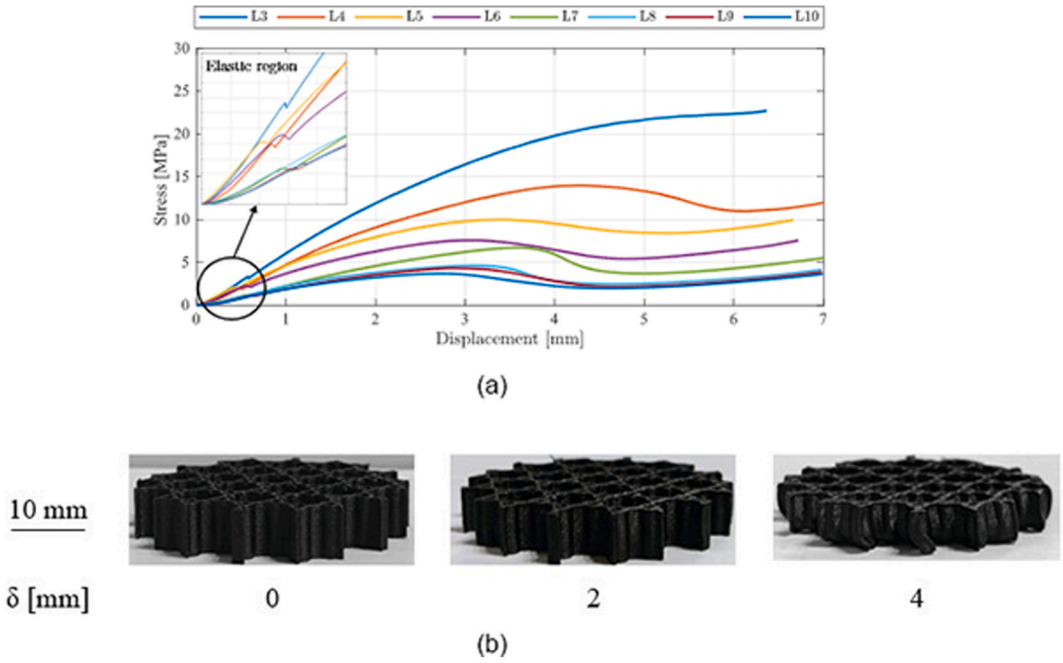

Fig. 5. Flatwise compressive behaviour according to ASTM C365. Representative stress-displacement curves for the different cell sizes (a); deformation sequence of the L6 specimen (b).

grid), and (iii) FG_CF (graded cells + boundary grid reinforced with continuous carbon fibre).

3.2. Plate twist test for cores

Under the plate-twist boundary conditions, all cores show a similar trend in the load–displacement response (Fig. 8): an initial linear rise followed by a progressive deviation from linearity and a smooth approach to a plateau, with no abrupt force drop. Across the entire displacement range, the ranking is consistent—FG_CF carries the highest load, FG is intermediate, and FG_noGrid the lowest—confirming the beneficial role of the boundary grid and, especially, of the continuous

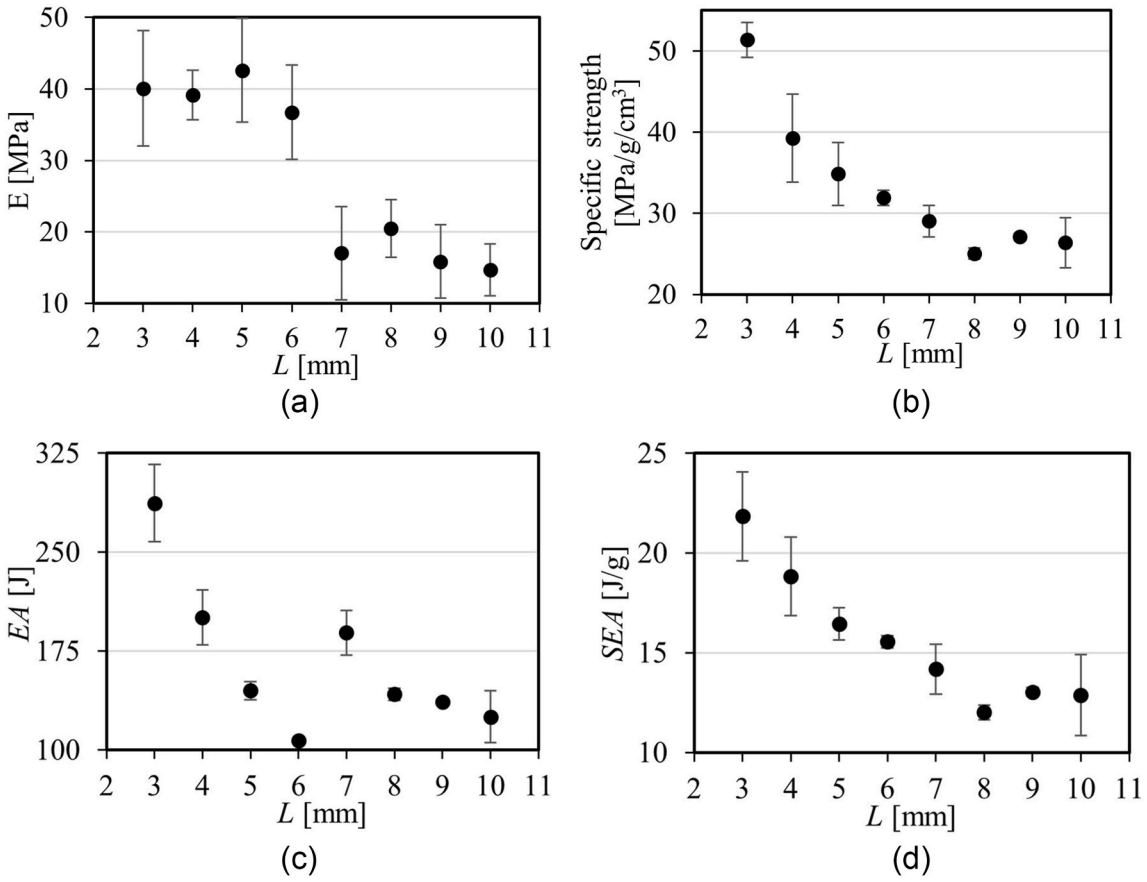

Fig. 6. Compression as a function of cell size *L*; stiffness (a), specific strength (b), energy absorption (*EA*) (c) and specific energy absorption (*SEA*) (d).

fibres embedded in it. The shaded bands in Fig. 8 indicate the repeatability of the tests (n = 3) and the small scatter relative to the mean curves. These observations are coherent with the compliance and twist-stiffness trends reported in Table 3.

Table 3 summarises mass, build time, and core-level metrics derived from the plate-twist test. At essentially the same build time (28 h) and with a small mass spread (72.7–74.8 g; ≤3%), the boundary grid and its fibre reinforcement deliver clear stiffness gains at negligible weight penalty. The compliance decreases from 0.16 ± 0.02 mm/N (FG_noGrid) to 0.13 ± 0.03 mm/N (FG, −19% vs FG_noGrid) and to 0.06 ± 0.01 mm/N (FG_CF, −62% vs FG_noGrid; −54% vs FG). Equivalently, the D_{66} increases from 7.35 ± 0.5 N m to 8.69 ± 0.4 N m (+18%) and to 18.5 ± 0.7 N m (+152% vs FG_noGrid; +113% vs FG). The same ranking (FG_CF > FG > FG_noGrid) is obtained for the equivalent core shear modulus (G_{12}) computed from the plate-twist formulation, confirming that the boundary grid improves load transfer across cell-size domains and that continuous fibres in the grid further amplify the effect.

3.3. Plate twist test for sandwich panel

A comparison of the core designs provides information about the potential of a functionally graded approach with the grid. Nonetheless, the entire sandwich still presents certain challenges related to the 3D-printed face sheets, and in particular regarding the interface strength of the core.

The representative load-displacement curves for each sandwich panel (Fig. 9a) demonstrated a continuous load increase until reaching the maximum. At this point, the panels broke, and the load dropped suddenly. In contrast to the core curves, which exhibited plateaus, the load-displacement curves of the sandwich panels did not plateau, with all panels demonstrating maximum displacements in excess of 15 mm. This behaviour is indicative of their fragile nature. Furthermore, the integrity of the core-to-face sheet interface was maintained throughout the testing process, suggesting that this interface is not the primary weakness of the sandwich panels.

The failure modes exhibited by the functionally graded designs were consistent each other (see Fig. 9b), manifesting as a crack initiation at the clamping point and subsequent propagation through the diagonal of the sample. In these cases, neither local deformation nor perforation was observed.

The quantitative results reported in Table 4 provide a comprehensive analysis of the studied core designs, including sandwich panels with functionally graded cores without grids, with grids, and with reinforced grids. The addition of face sheets serves to balance the differences at the core level (Table 4). The sandwich with a fibre-reinforced grid shows a ~46% lower compliance than FG_noGrid (≈+85% stiffness) and ~46% lower compliance than FG (≈+85% stiffness). This outcome serves to demonstrate the beneficial effect of embedding continuous carbon fibres into the grid. However, a comparison of sandwiches with and without a grid did not reveal any improvements in compliance. The Onyx® grid alone produces a negligible change in compliance (4.89 → 4.87 μm/N), whereas adding fibres produces a substantial reduction (to 2.64 μm/N).

3.4. Quantitative synthesis

To isolate the contribution of the face sheets and quantify the benefit of the sandwich architecture, the core-level and panel-level responses were compared under the same plate-twist boundary conditions (Fig. 3). Sandwich compliance values from Table 4—originally expressed in μm/N—were converted to mm/N to enable direct comparison with the core data shown in Table 3. This analysis aligns with the theoretical plate-twist formulation, in which torsional stiffness (the D_{66} term) is

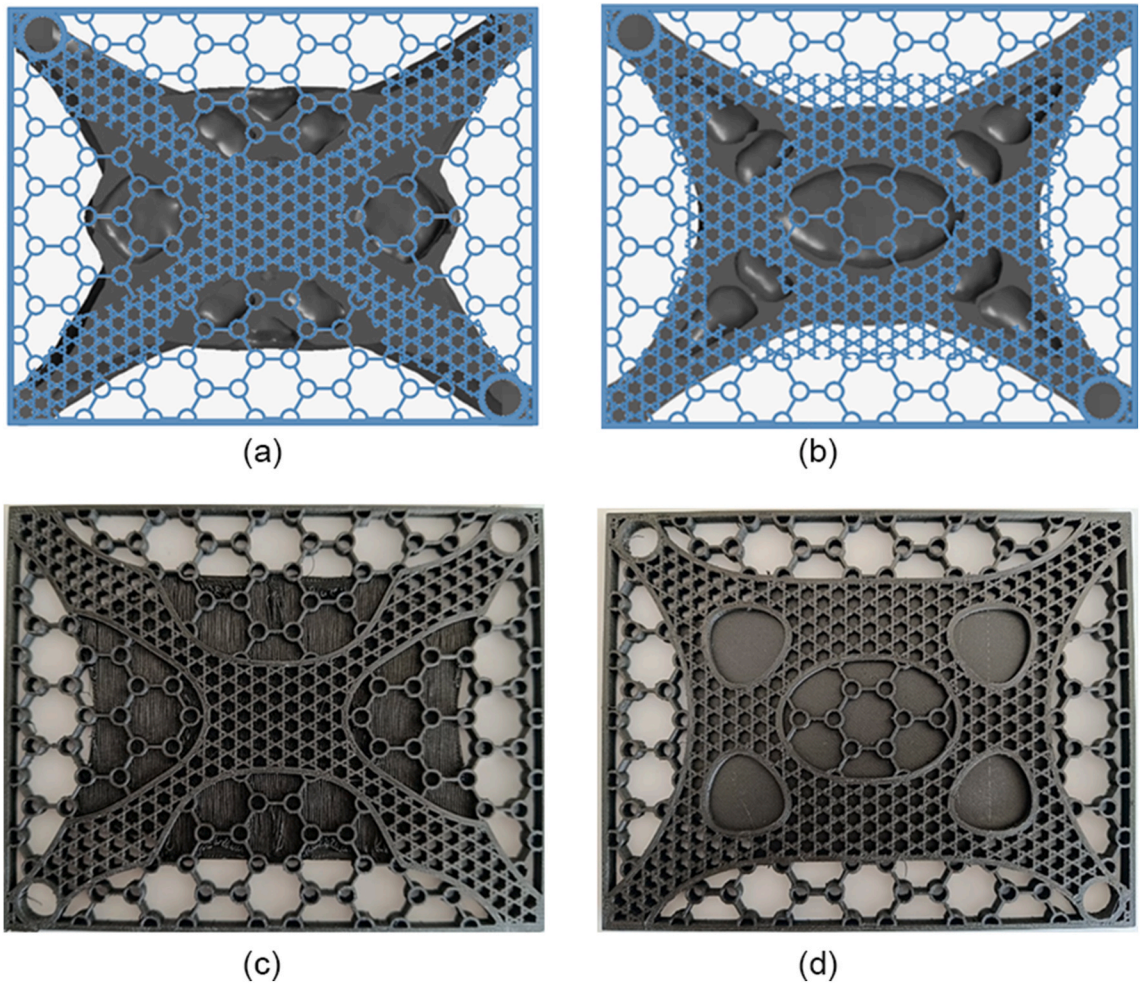

Fig. 7. Mapping the topology-optimised material distribution to the architected graded core. Upper half (tension side) (a), Lower half (compression side) (b), Printed core views of the corresponding halves (c–d).

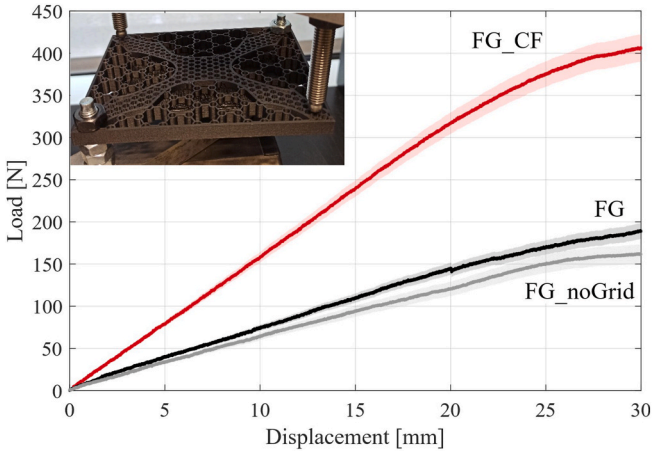

Fig. 8. Plate-twist load–displacement curves for the three core designs. Solid lines show the mean response, and the shaded band indicates the deviation.

primarily governed by the face sheets, while the core contributes predominantly through transverse shear stiffness. Summarised in Table 5.

Incorporating the integrally printed 1.5 mm face sheets results in a compliance reduction by a factor of approximately 23–33 across the three core designs, representing more than an order-of-magnitude increase in torsional stiffness. Even when accounting for the additional mass of the face sheets, the mass-normalized stiffness improves significantly, yielding a specific stiffness gain of roughly 11–17. This demonstrates the decisive efficiency advantage of the sandwich configuration for lightweighting applications.

Table 3
Summary of the tested core results.

	FG_noGrid	FG	FG_CF
Mass [g]	72.7 ± 0.5	73.1 ± 0.8	74.8 ± 1.7
Time [h]	28	28	28
C = δ/P [mm/N]	0.16 ± 0.02	0.13 ± 0.03	0.06 ± 0.01
D_{66c} [Nm]	7.35 ± 0.5	8.69 ± 0.4	18.5 ± 0.7

The sandwich with a fibre-reinforced grid exhibits a compliance of 2.64 μm/N, representing an improvement by a factor of approximately 1.85 relative to the unreinforced FG panel. In contrast, adding an Onyx® grid without fibres yields no appreciable benefit at the panel scale (4.89 → 4.87 μm/N). This is expected, as torsional stiffness at the panel scale is dominated by the face sheets, making the added stiffness of the Onyx® grid comparatively insignificant.

Across all sandwich variants, failure occurred through cracking of the face sheets, with no observed debonding between face sheets and core. This confirms one of the central advantages of integral 3D printing: the elimination of the traditional adhesive interface, which is typically the weakest point in conventionally manufactured sandwich structures. In this work, both the continuous fibre-reinforced grid and the

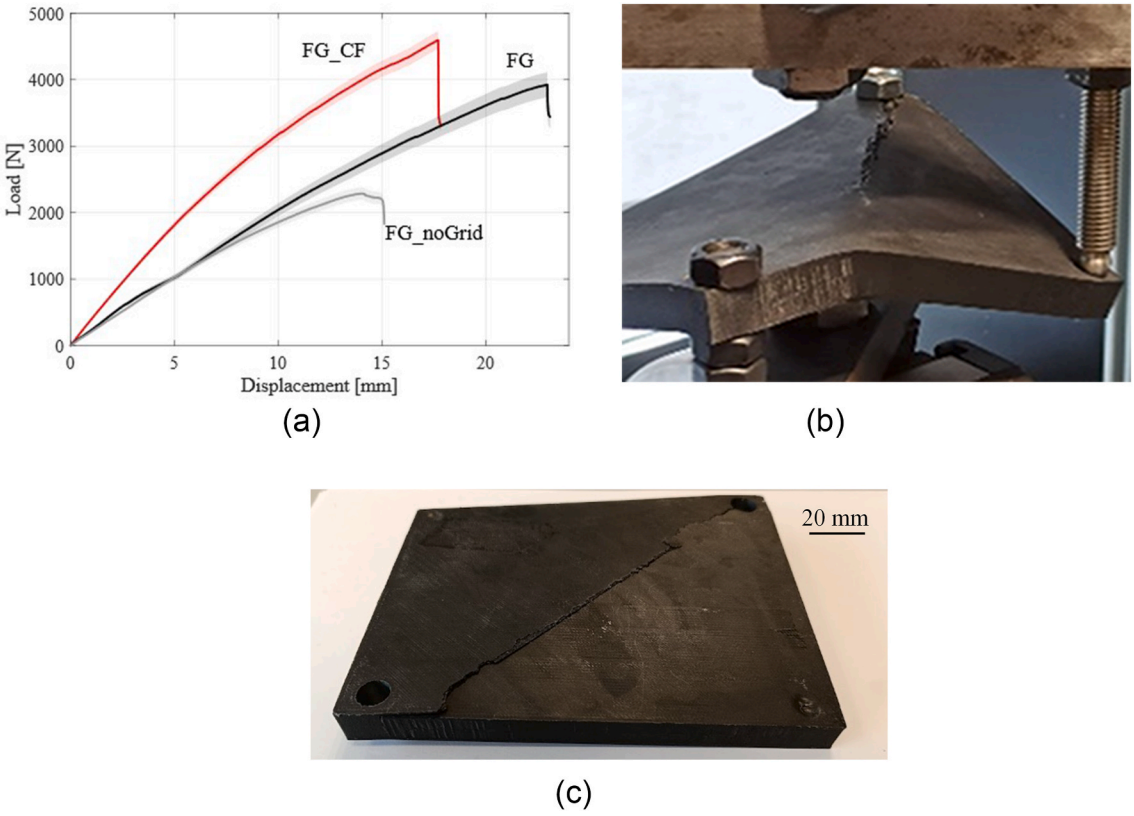

Fig. 9. Load-displacement curves of sandwich panels with functionally graded cores(a). Detail of the failure mechanism in the sandwich panel during test (b). Detail of the failure mechanism after test functionally graded core (c).

Table 4
Summary of the tested sandwich panel results.

	FG_noGrid	FG	FG_CF
Mass [g]	144 ± 1.5	145 ± 1.9	149 ± 2.7
Time [h]	37	37	37
C = δ/P [μm/N]	4.89 ± 0.5	4.87 ± 0.3	2.64 ± 0.3
Strength [kN]	2.28 ± 0.3	4.07 ± 0.1	4.37 ± 0.3

Table 5
Core vs. sandwich performance synthesis (plate-twist). (Compliance C = displacement per unit load; stiffness $= 1/C$; "specific stiffness gain" = (sandwich stiffness per kg) ÷ (core stiffness per kg).).

	Core C [mm/N]	Sandwich C [10^{-3} mm/N]	Stiffness gain [−]	Specific stiffness gain
FG_noGrid	0.16	4.89	32.72	16.52
FG	0.13	4.87	26.69	13.46
FG_CF	0.06	2.64	22.73	11.41

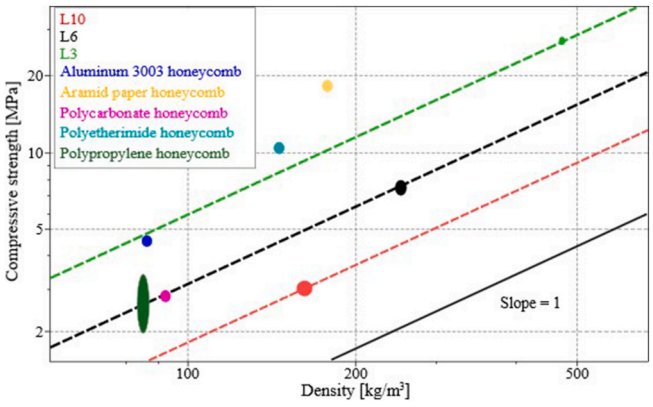

Fig. 10. Ashby chart comparing compressive strength and density for various commercial and printed core structures.

monolithic manufacture contribute to the preservation of geometric and mechanical continuity across the structure.

While the plate-twist test confirms the stiffness benefits of the FG sandwich assembly, the viability of the design ultimately depends on the load-bearing capacity of the constituent core cells. To validate this, Fig. 10 benchmarks the compressive strength of the printed trabecular architectures (L3, L6, L10) against standard commercial cores.

The comparison highlights several noteworthy trends. First, the L3 trabecular core achieves compressive strength levels comparable to, and in some cases exceeding, those of polymer-based commercial honeycomb cores, despite being manufactured entirely through material-extrusion 3D printing. Its position on the chart reflects an efficient balance between strength and density, demonstrating that architected microstructures can offset the relatively low stiffness of thermoplastic materials. The L6 configuration, while slightly lower in strength than L3, remains competitive with mid-density commercial polymer cores, confirming that intermediate cell sizes retain favourable load-bearing capability while reducing mass. In contrast, the L10 variant falls within the performance envelope of lightweight polypropylene or aramid-paper honeycombs, which is consistent with its reduced relative density and intentionally weight-minimised architecture. Overall, the distribution of the three printed designs across the strength–density domain shows that tailored trabecular architectures can span a broad range of mechanical performance—covering the functional space between lightweight polymer honeycombs and higher-density engineered cores—while offering the additional advantages of integral manufacturability and design freedom.

4. Conclusions

This study successfully demonstrates a multi-scale design and manufacturing strategy for high-performance, integrally 3D-printed sandwich panels. By combining a functionally graded honeycomb core with a continuous carbon fibre-reinforced grid, the structural performance was significantly enhanced, achieving a 52% increase in strength compared to unreinforced graded cores. The transition from core-level to panel-level analysis revealed a decisive efficiency gain, with the sandwich configurations providing up to a 17-fold increase in specific stiffness. Crucially, the integral manufacturing approach—printing the face sheets and hybrid core in a single process—successfully eliminated the traditional weak point of adhesive debonding. This resulted in a shift in the failure mode from the core-face interface to the face sheets themselves, ensuring maximum utilization of the material's structural capacity.

The proposed biomimetic methodology, which integrates topology optimisation with multi-material additive manufacturing, offers a robust framework for developing lightweight components tailored to complex loading conditions. By exploiting the design freedom of 3D printing, it is possible to achieve geometric and mechanical continuity across hierarchical scales, from the local cellular grading to the global panel reinforcement. This approach not only improves weight efficiency but also streamlines production by removing the need for secondary bonding processes. Ultimately, the successful validation of these hybrid sandwich structures under plate-twist conditions proves that this design-to-manufacturing workflow is a versatile and scalable solution for the next generation of high-performance structural applications.

CRediT authorship contribution statement

Itxaro Sukia: Writing – review & editing, Writing – original draft, Software, Investigation. **Aritz Esnaola:** Writing – review & editing, Validation, Supervision, Methodology. **Unai Morales:** Investigation. **Jon Aurrekoetxea:** Writing – review & editing, Supervision, Methodology.

Declaration of competing interest

The authors declare that they have no known competing financial interests or personal relationships that could have appeared to influence the work reported in this paper.

Acknowledgement

We would like to thank the Basque Government [IT1613-22; KK-2021/00066] and the European Commission [EU4DUAL, ERASMUS-EDU-2022-EUR-UNIV, Grant Agreement No. 101089937] for their financial support of this study.

Data availability

No data was used for the research described in the article.

References

[1] B. Castanie, C. Bouvet, M. Ginot, Review of composite sandwich structure in aeronautic applications, Composites Part C 1 (2020) 100004, https://doi.org/10.1016/j.jcomc.2020.100004.
[2] M.F. Aly, K.T. Hamza, M.M. Farag, A materials selection procedure for sandwiched beams via parametric optimization with applications in automotive industry, Mater. Des. 56 (2014) 219–226, https://doi.org/10.1016/j.matdes.2013.10.075.
[3] V. Birman, G.A. Kardomateas, Review of current trends in research and applications of sandwich structures, Compos. B Eng. 142 (2018) 221–240, https://doi.org/10.1016/j.compositesb.2018.01.027.
[4] Y. Li, R. Luo, W. Zhai, S. Shi, Y. Gao, Y. Liu, qi Zou, C. Zhang, Q. Han, A high impact resistant coupling bionic asymmetric sandwich panel inspired by red-eared turtle shell and coelacanth fish, Compos. Commun. 54 (2025), https://doi.org/10.1016/j.coco.2025.102281.
[5] T.A. Schaedler, W.B. Carter, Architected cellular materials, Annu. Rev. Mater. Res. 46 (2016) 187–210, https://doi.org/10.1146/ANNUREV-MATSCI-070115-031624/CITE/REFWORKS.
[6] Q. Zhang, X. Yang, P. Li, G. Huang, S. Feng, C. Shen, B. Han, X. Zhang, F. Jin, F. Xu, T.J. Lu, Bioinspired engineering of honeycomb structure - using nature to inspire human innovation, Prog. Mater. Sci. 74 (2015) 332–400, https://doi.org/10.1016/j.pmatsci.2015.05.001.
[7] N.S. Ha, G. Lu, A review of recent research on bio-inspired structures and materials for energy absorption applications, Compos. B Eng. 181 (2020) 107496, https://doi.org/10.1016/j.compositesb.2019.107496.
[8] X. Yu, Q. Zhang, M. Schenk, F. Scarpa, The engineering elastic constants of bio-inspired sandwich cores with wavy cylinders, Compos. Commun. 48 (2024), https://doi.org/10.1016/j.coco.2024.101893.
[9] Q. Ma, M.R.M. Rejab, Y. Song, X. Zhang, M.M. Hanon, M.H. Abdullah, A.P. Kumar, Effect of infill pattern of polylactide acid (PLA) 3D-printed integral sandwich panels under ballistic impact loading, Mater. Today Commun. 38 (2024) 107626, https://doi.org/10.1016/J.MTCOMM.2023.107626.
[10] S. Shi, Z. Sun, X. Hu, H. Chen, Flexural strength and energy absorption of carbon-fiber–aluminum-honeycomb composite sandwich reinforced by aluminum grid, Thin-Walled Struct. 84 (2014) 416–422, https://doi.org/10.1016/J.TWS.2014.07.015.
[11] S. Shi, B. Chen, Z. Sun, Equivalent properties of composite sandwich panels with honeycomb–grid hybrid core, J. Sandw. Struct. Mater. 22 (2020) 1859–1878, https://doi.org/10.1177/1099636218789615.
[12] Z. Sun, S. Shi, X. Guo, X. Hu, H. Chen, On compressive properties of composite sandwich structures with grid reinforced honeycomb core, Compos. B Eng. 94 (2016) 245–252, https://doi.org/10.1016/j.compositesb.2016.03.054.
[13] Z. Sun, D. Li, W. Zhang, S. Shi, X. Guo, Topological optimization of biomimetic sandwich structures with hybrid core and CFRP face sheets, Compos. Sci. Technol. 142 (2017) 79–90, https://doi.org/10.1016/j.compscitech.2017.01.029.
[14] H. Lv, S. Shi, B. Chen, J. Ma, Z. Sun, Low-velocity impact response of composite sandwich structure with grid–honeycomb hybrid core, Int. J. Mech. Sci. 246 (2023) 108149, https://doi.org/10.1016/j.ijmecsci.2023.108149.
[15] A. Casalotti, F. D'Annibale, G. Rosi, Multi-scale design of an architected composite structure with optimized graded properties, Compos. Struct. 252 (2020) 112608, https://doi.org/10.1016/j.compstruct.2020.112608.
[16] J. Grünewald, P. Parlevliet, V. Altstädt, Manufacturing of thermoplastic composite sandwich structures: a review of literature, J. Thermoplast. Compos. Mater. 30 (2017) 437–464, https://doi.org/10.1177/0892705715604681.
[17] F. Wang, Y. Ming, Y. Zhao, F. Yang, J. Lou, Y. Zhu, Y. Duan, B. Wang, H. Xiao, Fabrication of a novel continuous fiber 3D printed thermoset all-composite honeycomb sandwich structure with polymethacrylimide foam reinforcement, Compos. Commun. 45 (2024) 101794, https://doi.org/10.1016/J.COCO.2023.101794.
[18] P. Cheng, Y. Peng, S. Li, Y. Rao, A. Le Duigou, K. Wang, S. Ahzi, 3D printed continuous fiber reinforced composite lightweight structures: a review and outlook, Compos. B Eng. 250 (2023), https://doi.org/10.1016/j.compositesb.2022.110450.
[19] G. Liu, Y. Xiong, L. Zhou, Additive manufacturing of continuous fiber reinforced polymer composites: design opportunities and novel applications, Compos. Commun. 27 (2021) 100907, https://doi.org/10.1016/J.COCO.2021.100907.
[20] Y. Wang, G. Zhang, H. Ren, G. Liu, Y. Xiong, Fabrication strategy for joints in 3D printed continuous fiber reinforced composite lattice structures, Compos. Commun. 30 (2022) 101080, https://doi.org/10.1016/J.COCO.2022.101080.
[21] M. Iragi, C. Pascual-González, A. Esnaola, C.S. Lopes, L. Aretxabaleta, Ply and interlaminar behaviours of 3D printed continuous carbon fibre-reinforced thermoplastic laminates; effects of processing conditions and microstructure, Addit. Manuf. 30 (2019), https://doi.org/10.1016/j.addma.2019.100884.
[22] C. Pascual-González, M. Iragi, A. Fernández, J.P. Fernández-Blázquez, L. Aretxabaleta, C.S. Lopes, An approach to analyse the factors behind the micromechanical response of 3D-printed composites, Compos. B Eng. 186 (2020), https://doi.org/10.1016/j.compositesb.2020.107820.
[23] A.W. Alshaer, D.J. Harland, An investigation of the strength and stiffness of weight-saving sandwich beams with CFRP face sheets and seven 3D printed cores, Compos. Struct. 257 (2021) 113391, https://doi.org/10.1016/j.compstruct.2020.113391.
[24] X. Yu, Q. Zhang, R.J. da Silva, T.H. Panzera, M. Schenk, F. Scarpa, The bending of 3D-printed bio-inspired sandwich panels with wavy cylinder cores, Thin-Walled Struct. 205 (2024), https://doi.org/10.1016/j.tws.2024.112538.
[25] F.N. Ainin, M.D. Azaman, M.S.A. Majid, M.J.M. Ridzuan, Effect of varying core density and material on the quasi-static behaviors of sandwich structure with 3D-printed hexagonal honeycomb core, Polym. Compos. 45 (2024) 9948–9964, https://doi.org/10.1002/pc.28450.
[26] K. Sugiyama, R. Matsuzaki, M. Ueda, A. Todoroki, Y. Hirano, 3D printing of composite sandwich structures using continuous carbon fiber and fiber tension, Compos. Part A Appl. Sci. Manuf. 113 (2018) 114–121, https://doi.org/10.1016/j.compositesa.2018.07.029.
[27] J. Feng, L. Yao, Z. Lyu, Z. Wu, G. Zhang, H. Zhao, Mechanical properties and damage failure of 3D-printed continuous carbon fiber-reinforced composite honeycomb sandwich structures with fiber-interleaved core, Polym. Compos. 44 (2023) 1980–1992, https://doi.org/10.1002/pc.27221.
[28] F. Wang, H. Wang, G. Wang, R. Fu, S. Guan, J. Zhou, Effects of internal configurations and its processing quality on compressive performance for 3D printed continuous fiber reinforced composites honeycomb sandwich, Thin-Walled Struct. 202 (2024), https://doi.org/10.1016/j.tws.2024.112046.
[29] M. Iragi, C. Pascual-González, A. Esnaola, U. Morales, J. Aurrekoetxea, C.S. Lopes, L. Aretxabaleta, Design, manufacturing and testing of 3D printed variable-stiffness

laminates for improved open-hole tensile behaviour, Addit. Manuf. 63 (2023), https://doi.org/10.1016/j.addma.2023.103418.
[30] F. Avilés, F. Couoh-Solis, L.A. Carlsson, A. Hernández-Pérez, A. May-Pat, Experimental determination of torsion and shear properties of sandwich panels and laminated composites by the plate twist test, Compos. Struct. 93 (2011) 1923–1928, https://doi.org/10.1016/j.compstruct.2011.02.001.
[31] I. Sukia, A. Esnaola, B. Erice, J. Aurrekoetxea, Impact behaviour of bio-inspired sandwich panels integrally manufactured from 3D printed continuous carbon fibre reinforced polyamide, Compos. Sci. Technol. 250 (2024) 110515, https://doi.org/10.1016/j.compscitech.2024.110515.
[32] M. Mohsenizadeh, F. Gasbarri, M. Munther, A. Beheshti, K. Davami, Additively-manufactured lightweight metamaterials for energy absorption, Mater. Des. 139 (2018) 521–530, https://doi.org/10.1016/j.matdes.2017.11.037.
[33] C. Bhat, A. Kumar, S.C. Lin, J.Y. Jeng, Design of tessellation based load transfer mechanisms in additively manufactured lattice structures to obtain hybrid responses, Addit. Manuf. 76 (2023) 103774, https://doi.org/10.1016/j.addma.2023.103774.
[34] C. Bhat, A. Kumar, S.C. Lin, J.Y. Jeng, Design, fabrication, and properties evaluation of novel nested lattice structures, Addit. Manuf. 68 (2023) 103510, https://doi.org/10.1016/j.addma.2023.103510.
[35] M.F. Ashby, The properties of foams and lattices, Philos. Trans. R. Soc. A Math. Phys. Eng. Sci. 364 (2005) 15–30, https://doi.org/10.1098/RSTA.2005.1678.